ACS APPLIED MATERIALS & INTERFACES

Research Article

www.acsami.org

Magnesium-Doped $Li_{1.2}[Co_{0.13}Ni_{0.13}Mn_{0.54}]O_2$ for Lithium-Ion Battery Cathode with Enhanced Cycling Stability and Rate Capability

Yan X. Wang, Ke H. Shang, Wei He, Xin P. Ai, Yu L. Cao,* and Han X. Yang

Hubei Key Lab. of Electrochemical Power Sources, College of Chemistry and Molecular Sciences, Wuhan University, Wuhan 430072, China

ABSTRACT: Mg-doped $Li[Li_{0.2-2x}Mg_xCo_{0.13}Ni_{0.13}Mn_{0.54}]O_2$ is synthesized by introducing Mg ions into the transition-metal (TM) layer of this layered compound for substituting Li ions through a simple polymer-pyrolysis method. The structural and morphological characterization reveals that the doped Mg ions are uniformly distributed in the bulk lattice, showing an insignificant impact on the layered structure. Electrochemical experiments reveal that, at a Mg doping of 4%, the $Li[Li_{0.16}Mg_{0.04}Co_{0.13}Ni_{0.13}Mn_{0.54}]O_2$ electrode can deliver a larger initial reversible capacity of 272 mAh g^{-1}, an improved rate capability with 114 mAh g^{-1} at 8 C, and an excellent cycling stability with 93.3% capacity retention after 300 cycles. The superior electrochemical performances of the Mg-doped material are possibly due to the enhancement of the structural stability by substitution of Li by Mg in the TM layer, which effectively suppresses the cation mixing arrangement, leading to the alleviation of the phase change during lithium-ion insertion and extraction.

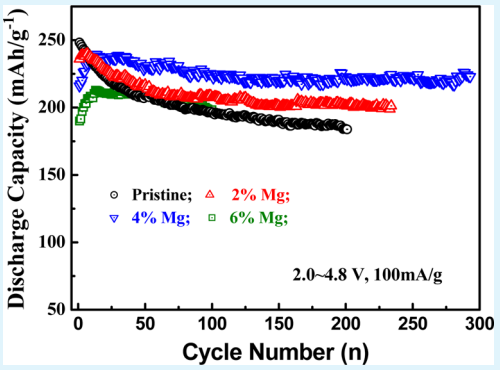

KEYWORDS: *magnesium doping, lithium-rich manganese-based oxides, cycling stability, rate capability, cathode, lithium-ion battery*

1. INTRODUCTION

Lithium-ion batteries (LIBs) with substantially enhanced energy density are now actively pursued as the most viable power sources for next-generation portable electronics, electric and hybrid vehicles, and even for grid-scale power storage applications.[1−5] To upgrade the specific energy of LIBs, it is a major challenge to find alternative cathodes with a similar cyclability but a greatly enhanced capacity than currently used cathodes. Among the various cathode materials being developed, the lithium-rich Mn-based oxides (LRMO), usually denoted as $xLi_2MnO_3\cdot(1-x)LiMO_2$ or $Li_{1+x/(x+2)}M_{(2-2x)/(x+2)}Mn_{2x/(x+2)}O_2$ (M = Mn, Ni, Co, etc.), are the most promising candidate, because of their high reversible capacity (~300 mAh g^{-1}), which is almost twice as high as those of the presently commercialized $LiCoO_2$ and $LiFePO_4$ cathodes in Li-ion batteries.[6−10]

Although the LRMO materials have the advantages of higher capacity and lower cost, they suffer from several disadvantages, such as low initial Coulombic efficiency and insufficient cyclability and rate capability, which impose a great obstacle for their practical applications. These shortcomings mainly originate from the unique electrochemical mechanism of the LRMO,[11,12] in which the LRMO must undergo an active process during the first charge in order to obtain an excessive reversible capacity.[13,14] This activation reaction gives a high-voltage plateau in the first charging curve, which is usually considered as the rearrangement of the transition-metal (TM) ions, because of the irreversible removal of Li_2O from its crystalline lattice. Despite this irreversible rearrangement of the TM ions, which can promote the electrochemical activity of Mn in Li_2MnO_3 to produce more reversible capacity below 3.5 V during the discharge, it results in a structural instability, leading to gradual capacity decay at cycling.[14−19] To solve these problems, many efforts have been contributed in the past decade to stabilize the surface and bulk phase structure of the LRMOs, thereby improving the initial Coulombic efficiency and cycling stability. One effective way is to modify the surface with inert oxides (Al_2O_3, TiO_2),[20,21] phosphates ($AlPO_4$, $CoPO_4$),[22,23] and fluorides (AlF_3).[24,25] The coating layers can really alleviate the side reaction of the electrolyte on the edge surface of the material, to decrease the initial irreversible capacity and protect the surface from attack by HF formed from the decomposition of the electrolyte.[26] Another approach to stabilize the crystal structure is to use the cation doping in the bulk phase. According to the matching principle of the ionic radius and the interstitial size of doping sites in the structure, the cation with the larger radius than Li ion (0.76 Å), such as Na ion (1.02 Å),[27] would be more suitable to occupy the sites in the Li layer. He et al. reported a Na-stabilized LRMO, which exhibited a high reversible capacity (307 mAh g^{-1}), rate capability (139 mAh g^{-1} at 8 C), and excellent cycling stability (89% capacity retention after 100 cycles), in comparison with its undoped counterpart, because the introduction of the Na ion into the bulk phase could expand the Li slab space to

Received: April 10, 2015
Accepted: May 26, 2015
Published: May 26, 2015

DOI: 10.1021/acsami.5b03125
ACS Appl. Mater. Interfaces 2015, 7, 13014−13021

improve the ionic diffusion kinetics.[28] For the cations with smaller radius than Li ion such as Al, Ti, Cr, Mo, Fe, and Ru ions,[29−34] these alien ions are believed to substitute Mn, Co, or Ni with comparable radius in the TM layer, resulting in an enhancement of the thermal and structural stability of the oxide material. Jiao et al. have employed Cr as an additional dopant to synthesize a series of Cr-doped $Li_{1.2}[Ni_{0.2-x/2}Mn_{0.6-x/2}Cr_x]O_2$ (x = 0, 0.02, 0.04, 0.06, and 0.08) samples, in which the Cr doping of x = 0.04 showed an improved capacity and rate capability, compared to the undoped sample, because of the reduced resistance of the electrode during cycling.[30] Park et al. reported that the substitution of Al^{3+} ions could prevent the structural degradation of the electrode material, allowing higher discharge capacities. The 6 mol% aluminum-doped $Li_{1.15}[Ni_{0.275-x/2}Mn_{0.575-x/2}Al_x]O_2$ electrode delivered approximately a discharge capacity of 210 mAh g^{-1} in a cutoff range between 2.5 V and 4.6 V, while the undoped electrode delivered an initial discharge capacity of 150 mAh g^{-1}. It was also found that the Al doping on $Li_{1.15}[Ni_{0.275-x/2}Mn_{0.575-x/2}Al_x]O_2$ material could decrease the area specific impedance (ASI).[33] Recently, Mg-doped lithium-rich oxide exhibited improving capacity (200 mAh g^{-1} at 20 mA g^{-1}), cycling performance (63% capacity retention up to 200 cycles) and rate capability (~120 mAh g^{-1} at 1000 mA g^{-1}), resulting from an expansion of the lattice, as a result of Mg doping.[35] Although the cation doping can improve the cycling stability, to some extent, it is still needed to enhance the cycling capability of these materials for battery applications. The insufficient electrochemical performance of these doped materials may result from how the multiple metal ions could be uniformly distributed in the entire preparation process, particularly for the trace doping ions. Therefore, a suitable approach is very crucial to develop high-performance cathode materials with the trace doping.

In our previous works,[20,28,36,37] we have adopted a polymer-pyrolysis method to prepare doped or nanosized oxide materials with homogeneously distributed multiple TM ions in the lattice. Compared to other methods,[38−41] such as the solid-state, coprecipitation, and sol−gel methods, the polymer-pyrolysis method is simple and particularly suitable for preparation of mixed metal oxides. In this work, we use this synthetic method to introduce the Mg ion into the TM layer of the LRMO material to substitute Li sites for stabilizing the bulk lattice and report the beneficial effect of the Mg doping on the long-term cycling performance of the LRMO material.

2. EXPERIMENTAL SECTION

2.1. Sample Preparation and Characterization. A simple polymer-pyrolysis method was used for the synthesis of the pristine sample $Li[Li_{0.2}Co_{0.13}Ni_{0.13}Mn_{0.54}]O_2$ (LRMO) and Mg-doped sample Li $[Li_{0.2-2x}Mg_xCo_{0.13}Ni_{0.13}Mn_{0.54}]O_2$ (x = 0.02, 0.04, and 0.06, denoted as 2%Mg-LRMO, 4%Mg-LRMO, and 6%Mg-LRMO, respectively). Stoichiometric amounts of $LiOH{\cdot}H_2O$, $Mg(NO_3)_2$, $Ni(NO_3)_2{\cdot}6H_2O$, $Co(NO_3)_2{\cdot}6H_2O$, and $Mn(NO_3)_2$ (50% aqueous solution) were first dissolved in the aqueous solution of acrylic acid. A small amount of $(NH_4)_2S_2O_8$ aqueous solution then was added to the mixed acrylic acid solution as an initiator to promote the polymerization. Under heating at 80 °C for ~3−5 h, the mixed solution was dried to form the well-distributed polyacrylates of Li, Mg, Ni, Co, and Mn. Afterward, the resulting polyacrylates were dried at 120 °C. The obtained copolymeric precursor was then decomposed at 480 °C for 5 h in air to give the powders of a Li-Ni-Co-Mn oxide precursor. The precursor powders then were calcined at 900 °C for 12 h in air to obtain the final product. A 5% excess of lithium was used to compensate for lithium loss during the calcinations.

Powder X-ray diffraction (XRD) (Bruker, Model D8 Avance) using Cu Kα radiation was used to identify the crystalline phase of the as-prepared powders and cycled electrodes. Rietveld refinement was then performed on the XRD data to obtain the lattice constants. The XRD spectra were collected in a range of 2θ values from 10°−80° at a scanning rate of 1° 2θ/min and a step size of 0.02° 2θ. The morphologies of the as-synthesized samples were observed by scanning electron microscopy (SEM) (Model JSM-6700F, JEOL, Japan) .

2.2. Electrochemical Measurements. The electrochemical properties of LRMO and Mg-LRMO were measured in 2016 coin-type cells with a Li metal anode. The electrolyte consisted of 1 M $LiPF_6$ in a mixture of ethylene methyl carbonate and ethylene carbonate at a 7:3 volume ratio. For fabrication of the cathodes, the as-synthesized powders were mixed with carbon black and polyvinylidene fluoride (80:10:10) in N-methylpyrrolidinone. The obtained slurry was coated onto Al foil and roll-pressed. The coin cells were assembled in an argon-filled glovebox. The galvanostatic charge−discharge tests were carried out on a battery measurement system (Model 2001T, Land, China) within a voltage range of 2.0−4.8 V vs Li^+/Li at room temperature. The cyclic voltammograms were measured by coin cell on an electrochemical station (CHI, Model 660a) at a scanning rate of 0.1 mV s^{-1} with the voltage ranging from 2.0 V to 4.8 V. Electrochemical impedance spectroscopy (EIS) measurements of all the samples were conducted at an open-circuit voltage in the frequency range of 100 kHz to 1 mHz with a voltage amplitude of 5 mV using a Model IM6 electrochemical impedance analyzer.

3. RESULTS AND DISCUSSION

3.1. Material Preparation and Characterization. Figure 1 shows the SEM images of the pristine LRMO and Mg-LRMO powders. As displayed in the images, all the LRMO powders show a similar morphology as nanoparticles with the size of 200−300 nm. However, the $Li[Li_{0.2-2x}Mg_xCo_{0.13}Ni_{0.13}Mn_{0.54}]$-

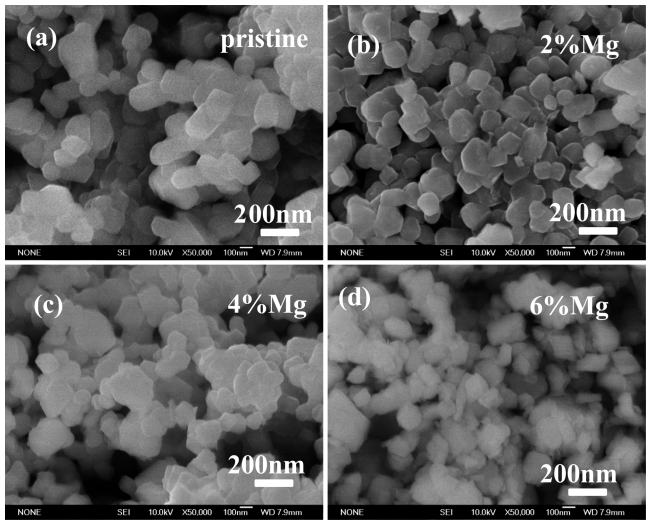

Figure 1. SEM images of (a) the pristine $Li[Li_{0.2}Mn_{0.54}Ni_{0.13}Co_{0.13}]O_2$ compound and $Li[Li_{0.2-2x}Mg_xMn_{0.54}Ni_{0.13}Co_{0.13}]O_2$ ((b) x = 0.02, (c) x = 0.04, and (d) x = 0.06).

DOI: 10.1021/acsami.5b03125
ACS Appl. Mater. Interfaces 2015, 7, 13014−13021

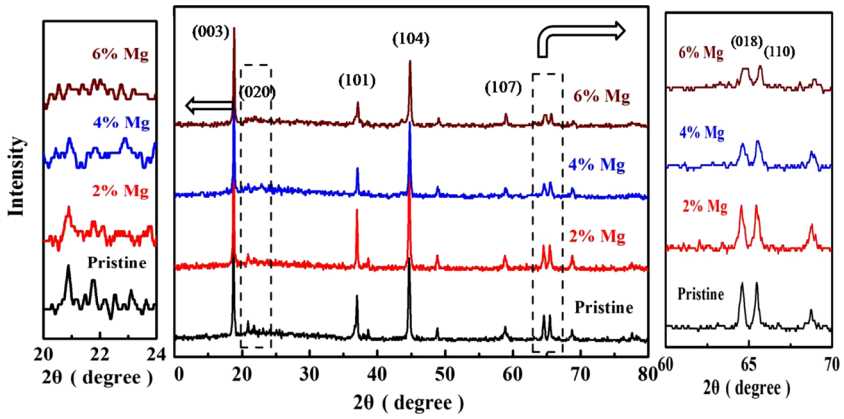

Figure 2. XRD patterns of the pristine and Mg-doped $Li[Li_{0.2-2x}Mg_xMn_{0.54}Ni_{0.13}Co_{0.13}]O_2$ (x = 0.02, 0.04, 0.06).

O_2 (x = 0, 0.02, and 0.04) samples appear as homogeneously distributed particles with well-defined morphologies, besides the 6%Mg-LRMO sample exhibits fuzzy shape to some extent. This could be explained that the Mg doping in the transition layer of the LRMO structure would hinder electron delocalization, leading to poor electron conductivity of the Mg-LRMO.

XRD patterns of the pristine LRMO and Mg-LRMO samples are displayed in Figure 2. The peaks in all the samples can be indexed as the O3-type layered structure (space group $R\bar{3}m$) with the additional weak reflections from a short-ranged superstructure at $2\theta \approx 20°-24°$, corresponding to the order occupation of Li, Mg, Mn, Ni atoms in the TM layers. No impurity phase can be detected in all samples, indicating that the Mg ion can be successfully doped into the crystal lattice, even at Mg doping amounts up to 6%. It is worth noting that some tiny differences in XRD pattern can be observed as the amount of Mg doping increases. The XRD peaks corresponding to a superstructured lattice at $2\theta \approx 20°-24°$ gradually decreased as the Mg doping amount increased, as shown in the left inset of Figure 2. This indicates that the Mg doping could impact the ordering of Li, Mn, Ni atoms in the TM layers, leading to the destruction of the superstructure. In addition, the splitting of the (018)/(110) peaks becomes weaker as the Mg doping amount increases, as shown in the right inset of Figure 2, suggesting that the introduction of Mg ions could effect the regularity of the layer structure. The phenomena could indicate, indirectly, the introduction of Mg ions into the TM layer of the lattice, because Mg cannot enter the Li layer in TM oxides, despite the similar ionic radii of Mg^{2+} and Li^+, as suggested by the Dahn group.[42,43]

3.2. Electrochemical Performance. Cyclic voltammetry (CV) measurements were carried out to compare the electrochemical redox responses of the Li-$[Li_{0.2-2x}Mg_xMn_{0.54}Ni_{0.13}Co_{0.13}]O_2$ (x = 0, 0.02 and 0.04) electrodes. As shown in Figure 3a, the CV curve of the pristine LRMO sample shows two oxidation peaks at ~3.9 V and ~4.6 V (vs Li^+/Li) in the initial anodic scan, which could be attributed to the oxidation of Ni^{2+} and Co^{3+} ions and the removal of lithium ions along with the simultaneous oxygen evolution, respectively.[28,44−46] In the reversal scan, a distinct reduction peaks occurs at ~3.3 V, corresponding to the Mn^{4+} reduction to balance the charge of oxygen vacancies arising from the loss of oxygen in the first charge process. However, the current peaks representing the reduction of Ni^{4+} and Co^{4+} were not observed apparently, suggesting the overlapping each other beneath the board peak in the potential region of 3.7−4.5 V. In contrast, the CV features of the Mg-LRMO samples (Figures 3b and 3c) showed some differences. First, although

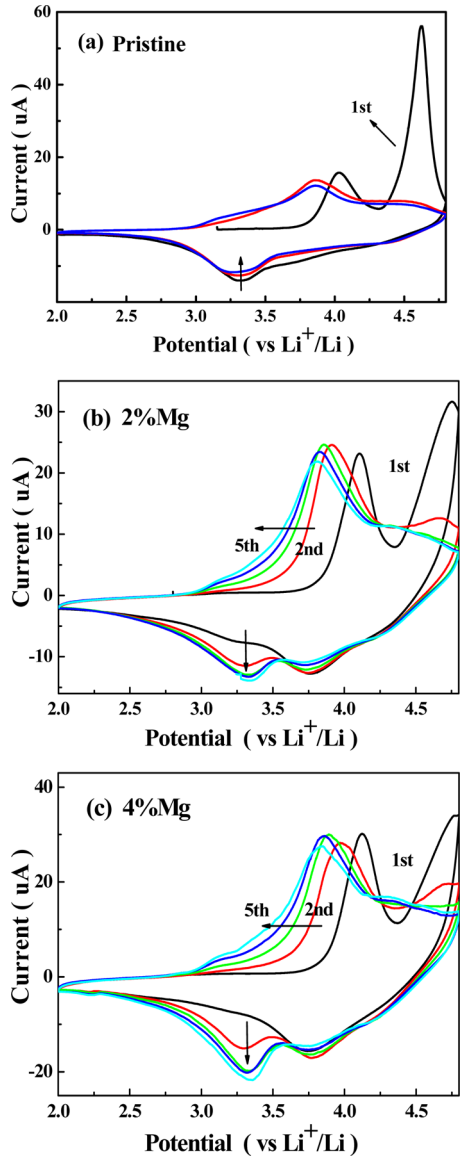

Figure 3. Cyclic voltammograms of (a) the pristine LRMO and (b,c) the Mg-LRMO electrode scanned at 0.1 mV s^{-1}.

DOI: 10.1021/acsami.5b03125
ACS Appl. Mater. Interfaces 2015, 7, 13014−13021

there were two oxidation peaks similar to those of the pristine LRMO sample in the first charge (Figure 3a), a distinct reduction peak appears at ~3.75 V, corresponding to the reduction of Ni^{4+} and Co^{4+}, which cannot be observed from the pristine LRMO sample (Figure 3a). This indicates that the Mg doping could improve the electrochemical reversibility of Ni^{4+}/Ni^{2+} and Co^{4+}/Co^{3+}. It can also be seen from the subsequent CV curves that the oxidation peaks of the Mg-doping samples shifts gradually toward negative potential and the reductive peak currents increase with increasing cycle number, pointing out the occurrence of an activation process in the initial cycles for the Mg-doping samples. The activation process shows that the electrochemical polarization decrease gradually in first several cycles, possibly due to the strong binding energy for Mg−O bond,[47] resulting in insufficient release in structure during Li ion insertion and extraction. Although the Mg-doping sample with strong bond energy exhibited higher electrochemical polarization, compared to the pristine sample, it would remain stable structure during cycling, thus leading to an enhanced cycling capability. In addition, it is also found that there is an apparent difference in the relative ratio of the oxidation peaks of the pristine and Mg-doping samples at first scan. If the ratio of the oxidation peak currents (I(4.6 V)/I(4.0 V)) is denoted as R, the R value is 3.24, 1.35, and 1.1 for the pristine LRMO, 2%Mg-LRMO, and 4%Mg-LRMO, respectively. Because the oxidation peak at ~4.6 V is attributed to an irreversible electrochemical reaction, the lower R value suggests an alleviated oxygen loss or decomposition of electrolyte at the high potential region. Therefore, this phenomenon suggests that the Mg doping may make less structural changes, to contribute to cycling stability, and alleviates the edge reaction of the electrolyte, to improve initial Coulombic efficiency.

Figure 4a presents the initial charge and discharge curves of the pristine LRMO and Mg-LRMO samples at the 0.1 C rate (30 mA g^{-1}). It can be seen that both of the samples exhibits similar charge/discharge characteristics: a sloping voltage profile under 4.5 V followed by a high-voltage plateau at 4.5 V during charging, in good agreement with the oxidation peaks at ~4.0 V and 4.6 V observed in CV curves (Figure 3), respectively. The corresponding initial charging/discharging data were summarized in Table 1. It can be observed that the reversible capacity of the Mg-LRMO electrodes decrease gradually with increasing Mg doping amount, while the capacity at voltage plateau at 4.5 V and the initial Coulombic efficiency have also similar tendencies. The results indicate that the relative decrease of the irreversible reaction at 4.6 V, as mentioned above from CV curves (Figure 3) cannot be simply ascribed to the decomposition of the electrolyte, because of low Coulombic efficiency for Mg-doping samples, but should also be contributed to the irreversible structural change. Although the decrease of the irreversible structural change with increasing Mg doping amount causes low reversible capacity of the electrode, it could make the layer structure less destroyed to improve cycling stability of the electrode. We can observe that the 6%Mg-LRMO electrode shows only a reversible capacity of 223 mAh g^{-1} and Coulombic efficiency of 73%, while the 2% Mg-LRMO and 4%Mg-LRMO electrodes still remain relatively high capacity and Coulombic efficiency, suggesting that the excess Mg doping possibly causes low electron conductivity, leading to a high electrochemical polarization.

In order to reveal the effect of Ni- and Li-substitution by Mg in the TM layer on the electrochemical performance, $Li[Li_{0.16}Mg_{0.02}Mn_{0.54}Ni_{0.13}Co_{0.13}]O_2$ (2%Mg-LRMO) and Li-

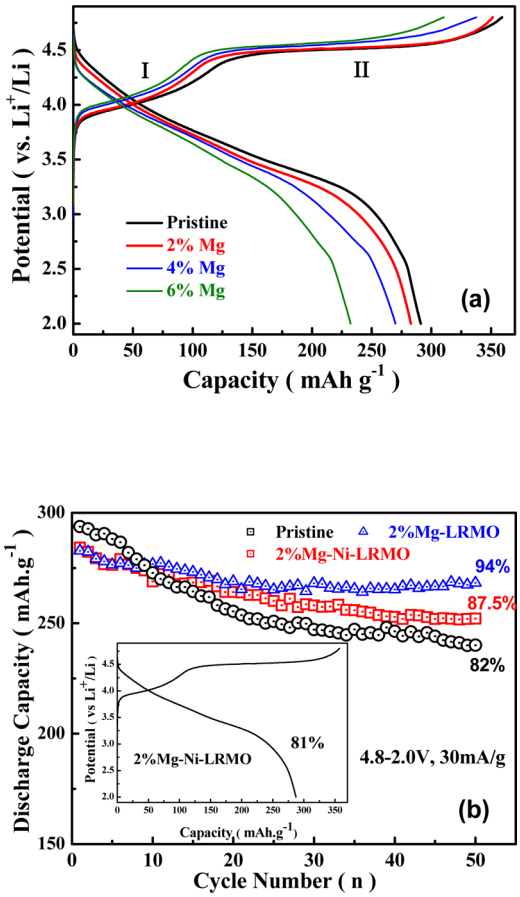

Figure 4. (a) Initial charge−discharge curves of the pristine LRMO and Mg-LRMO samples at 0.1 C (30 mA g^{-1}). (b) The cycling performance of the pristine LRMO, 2%Mg-LRMO, and 2%Mg−Ni-LRMO samples at 0.1 C. Inset shows the initial charge−discharge curve of the 2%Mg−Ni-LRMO sample.

Table 1. Initial Charge/Discharge Data of $Li[Li_{0.2-2x}Mg_xMn_{0.54}Ni_{0.11}Co_{0.13}]O_2$ (x = 0, 0.02, 0.04, 0.06)

sample	charging capacity (mAh g^{-1})	discharging capacity (mAh g^{-1})	capacity of the voltage plateau at 4.5 V (mAh g^{-1})	initial Coulombic efficiency (%)
LRMO	364	291	235	80
2%Mg	352	285	218	81
4%Mg	348	272	210	78
6%Mg	304	223	180	73
2%Mg−Ni	356	288	231	81

$[Li_{0.2}Mg_{0.02}Mn_{0.54}Ni_{0.11}Co_{0.13}]O_2$ (2%Mg−Ni-LRMO) samples were prepared and their electrochemical performance were investigated by charging/discharging measurement at 0.1 C (30 mA g^{-1}), as shown in Figure 4b. As can be seen, the 2%Mg−Ni-LRMO electrode can deliver similar reversible capacity (288 mAh g^{-1}) and initial Coulombic efficiency (81%), compared to those (284 mAh g^{-1}, 81%) of the 2%Mg-LRMO electrode. However, the capacity retention (87.5%) of the 2%Mg−Ni-LRMO electrode is much less than that (94%) of the 2%Mg-LRMO electrode after 100 cycles, indicating that the substitution Li by Mg in the TM layer is more effective for the structural stabilization during cycling than the substitution Ni by Mg. This result can be possibly explained that the

DOI: 10.1021/acsami.5b03125
ACS Appl. Mater. Interfaces 2015, 7, 13014−13021

substitution Li by Mg in the TM layer could effectively prevent Li ion migrating from the TM layer to the Li slab layer, to suppress the phase transfer from a layered to a spinel structure. In fact, no matter which substitution of Li or Ni by Mg in the TM layer, the Mg-doped materials showed better cycling stability than the pristine material (Figure 4b). Based on the above discussion, we further investigated the electrochemical performance of the materials with the Li-substitution by Mg.

To further study the effect of Mg doping on the cycling stability, the pristine LRMO electrode and Mg-LRMO electrodes were cycled between 2.0 and 4.8 V at 1/3 C (100 mA g^{-1}). As shown in Figure 5, an interesting phenomenon can

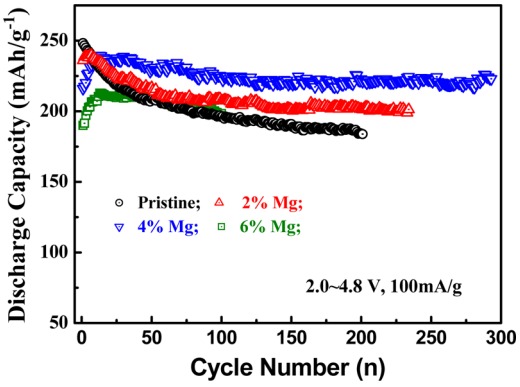

Figure 5. Cycle performances of the pristine LRMO and Mg-LRMO electrodes between 2.0 and 4.8 V at 1/3 C (100 mA g^{-1}).

be observed. The cycling capacities of the samples with a low amount of Mg doping (0% and 2%) first decline and then remain stable, while the cycling capacity of the sample with higher Mg doping (4% and 6%) first increase and then remain stable, which demonstrate sufficiently that a high Mg doping amount could cause high cation mixing (Li^+, Mg^{2+}, Ni^{2+}),[48,49] which suppress Li ion insertion and extraction. After the initial activation process, the electrodes delivered a stable capacity with the decreased electrochemical polarization, in good agreement with the observation of the CV curves (Figure 3). Among these samples, the 4%Mg-LRMO electrode showed higher cycling capacity (223 mAh g^{-1} after 300 cycles) and capacity retention (93.3% after 300 cycles, even relative to the maximum cycling capacity), corresponding to low capacity decay ratio of 0.02% per cycle. The greatly enhanced cycling capability for the Mg-LRMO electrode is because the presence of Mg ion can stabilize the crystal structure, to inhibit effectively phase transfer during cycling.

Figure 6 gives the rate capability of the pristine LRMO and Mg-LRMO electrodes under galvanostatic charge and discharge test at different rates from 0.1 C to 8 C (1 C = 300 mA g^{-1}). The relative rate data were summarized in Table 2. Although the 2%Mg-LRMO and 4%Mg-LRMO electrodes showed lower reversible capacity at 0.1 C, compared to the pristine LRMO electrode, they delivered a discharge capacity of 124 and 112 mAh g^{-1} at 8 C, which are higher than that of the pristine LRMO electrode (104 mAh g^{-1}). Such excellent rate capability of the 2%Mg-LRMO and 4%Mg-LRMO electrodes might be attributed to the activation process that creates a favorable chemical composition and structure for the high rate charge/discharge (Figure 5). However, the 6%Mg-LRMO electrode exhibited very poor rate capability, indicating that the excessive doping could result in severe cation mixing arrangement in the

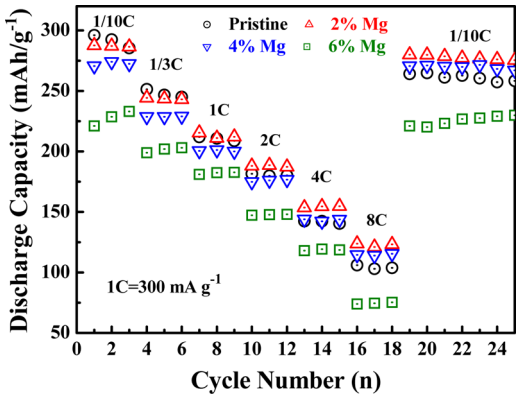

Figure 6. Rate capability performances of the pristine LRMO and Mg-LRMO electrodes. The charging/discharging rates are the same.

Table 2. Reversible Capacity of $Li[Li_{0.2-2x}Mg_xMn_{0.54}Ni_{0.13}Co_{0.13}]O_2$ (x = 0, 0.02, 0.04, 0.06) at Various Rates

	Capacity (mAh g^{-1})					
	1/10 C	1/3 C	1 C	2 C	4 C	8 C
LRMO	291	251	210	181	149	103
2%Mg-LRMO	285	244	212	187	154	124
4%Mg-LRMO	272	229	200	174	144	114
6%Mg-LRMO	221	201	182	147	119	75

TM layer, which reduces the electron conductivity and causes sluggish kinetics. So, the appropriate amount of Mg doping is very important to develop highly stable and high-rate-capable LRMO material. This work suggests the 2%−4% Mg doping is of a good choice. It is noteworthy that, when the current was reduced back to 0.1 C, the discharge capacities of the Mg-doping electrode can almost recover its initial capacity value, while the pristine LRMO electrode returns to only 89% of its initial capacity. This phenomenon indicates that the Mg-doped LRMO material may tolerate the impact of high current density and guarantee the structural stability at various rates.

EIS is a powerful technology to detect the changes of the electrode resistance inside the cell, including solid electrolyte interface (SEI) film and charge-transfer reaction. EIS spectra of the pristine LRMO and 4%Mg-LRMO electrodes cycled at different cycles are performed and shown in Figure 7. All the Nyquist plots are composed of two depressed semicircles and a slope.[28,50] The semicircle in the high-frequency region is associated with the surface film resistance (R_f) formed by the decomposition of the electrolyte in the high-voltage range. The semicircle in the middle frequency region represents the charge-transfer resistance (R_{ct}) due to the Li insertion reaction. The slope in the low-frequency region corresponds to a diffusion-controlled process of the lithium ion in the bulk. Based on the equivalent circuit given in the inset of Figure 7, the value of R_{ct} and R_f are simulated and listed in the inset of Figure 7. As shown, in the second cycle, the R_f and R_{ct} values (101 and 447 Ω, respectively) for the 4%Mg-LRMO electrode are found to be similar to those (109 and 417 Ω, respectively) for the pristine LRMO electrode. After 30 cycles, for the pristine LRMO electrode, the R_f value increased slightly from 101 Ω in the second cycle to 120 Ω, while the R_{ct} value almost doubled, from 447 Ω in the second cycle to 741 Ω, indicating that the pristine LRMO underwent continuous phase change with cycling, leading to structural instability on the surface and in the bulk phase of the material. However, for the 4%Mg-

DOI: 10.1021/acsami.5b03125
ACS Appl. Mater. Interfaces 2015, 7, 13014−13021

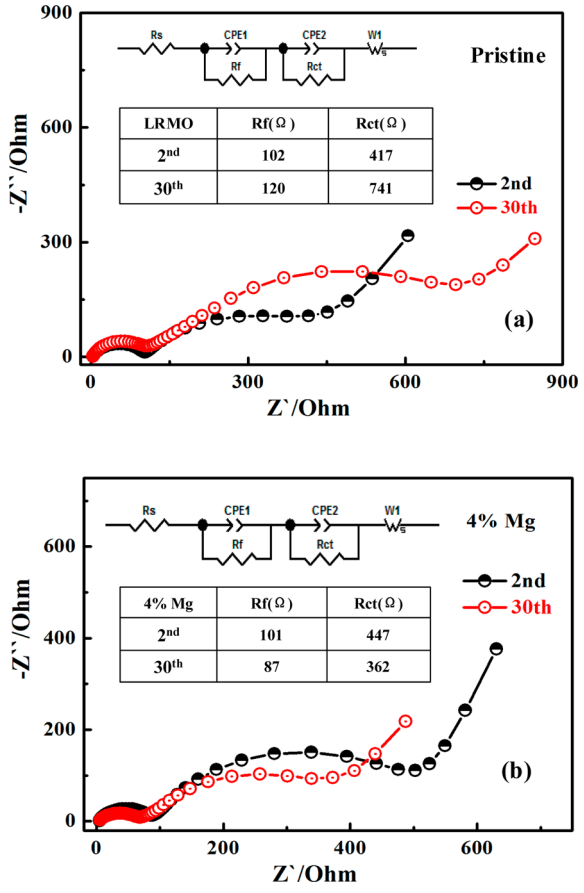

Figure 7. EIS plots of (a) the pristine LRMO and (b) the 4%Mg-LRMO electrodes (b). The insets show the equivalent circuit and the corresponding data.

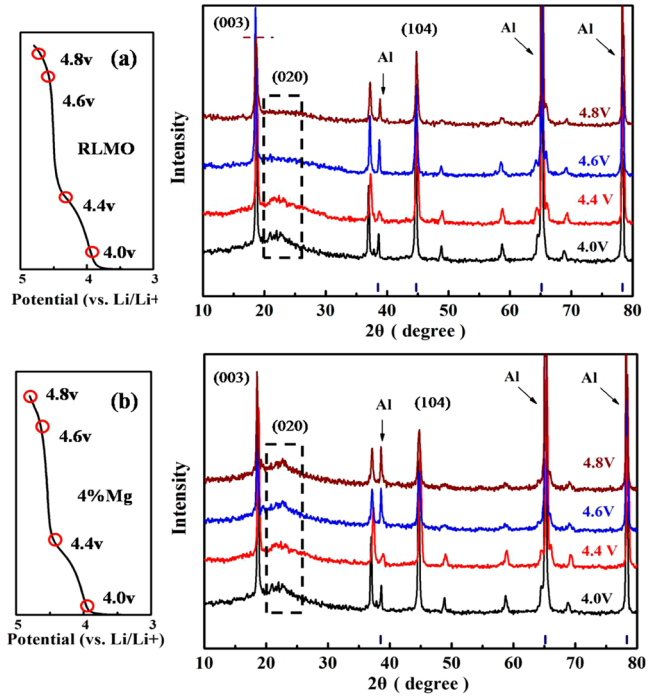

Figure 8. *Ex situ* XRD patterns of (a) the pristine LRMO and (b) Mg-LRMO electrodes at different charging stages.

LRMO electrode, the R_f and R_{ct} values were found to decrease slightly after 30 cycles, revealing that the Mg doping electrode could effectively suppress phase change with cycling. The decreased R_{ct} value demonstrated that the Mg-doped sample underwent an initial active process to decrease the electrochemical polarization, in accordance with the observations in Figures 3 and 5. The decreased R_{ct} value for the 4%Mg-LRMO electrode also contributed a high rate capability, as shown in Figure 6.

To understand the impact of the Mg doping on the structural stability of the LRMO material more clearly, the structural change is evidenced by the *ex situ* XRD experiment. Figure 8 shows the XRD patterns of the pristine LRMO and 4%Mg-LRMO electrodes at different charging stages. It is clearly observed that the XRD peaks at $2\theta \approx 20°-24°$, corresponding to a monoclinic superstructure, gradually disappeared with the progress of charging (Figure 8a), indicating that the superstructure was destroyed because of the occurrence of the large phase change during charging. However, the XRD peaks at $2\theta \approx 20°-24°$ of the 4%Mg-LRMO electrode can still be observed, even when charged to 4.8 V (Figure 8b), suggesting that the superstructure still remains at the end of charging. These results demonstrate that, apparently, the excellent cycling performance of the Mg doping samples should be ascribed to enhanced structural stability by Mg doping.

4. CONCLUSIONS

In summary, Mg-doped LRMO cathode materials are prepared via a simple polymer-pyrolysis method. The XRD results suggest that Mg ions can be introduced uniformly into the crystalline lattice to substitute Li in the TM layer, even at doping amounts up to 6%. The charge−discharge measurements demonstrate that the Mg-LRMO electrodes have slightly low reversible capacity and show an electrochemical activation process in initial several cycles, indicating that the Mg doping can hinder metal ion mixing arrangement to some extent and increase the electrochemical polarization. Although the Mg-doping materials all exhibit better cycling stability, compared to the pristine LRMO, taking into account the balance in reversible capacity, rate, and cycling capability, the Li-$[Li_{0.16}Mg_{0.04}Co_{0.13}Ni_{0.13}Mn_{0.54}]O_2$ electrode is the optimal choice, with a large initial reversible capacity (272 mAh g^{-1}), improved rate capability (114 mAh g^{-1} at 8 C), and excellent cycling stability (93.3% capacity retention after 300 cycles, even relative to the maximum cycling capacity). The improved electrochemical performances of the Mg-doped material are attributed to the contribution of the Mg doping in the bulk lattice, which can effectively enhance the structural stability. Therefore, the Mg doping is a facile and effective approach to improve the cycling performance of the Li-rich layered metal oxides for Li-ion battery applications.

AUTHOR INFORMATION

Corresponding Author

*Tel.: 86-027-68754526. E-mail: ylcao@whu.edu.cn.

Author Contributions

All authors contributed equally to this work. Y.L.C. conceived the idea of Mg-doped Li-rich layered metal oxides; Y.X.W., K.H.S., and W.H. directed the experimental work and conducted the measurements. Y.L.C. and H.X.Y. wrote the paper; all authors participated in the analysis of the

DOI: 10.1021/acsami.5b03125
ACS Appl. Mater. Interfaces 2015, 7, 13014−13021

experimental data and discussions of the results, as well as preparing the paper.

Notes

The authors declare no competing financial interest.

■ ACKNOWLEDGMENTS

We thank financial support by the National Key Basic Research Program of China (No. 2015CB251100), National Science Foundation of China (Nos. 21173160, 21333007) and, Program for New Century Excellent Talents in University (No. NCET-12-0419) and Hubei National Funds for Distinguished Young Scientists (No. 2014CFA038).

■ REFERENCES

(1) Armand, M.; Tarascon, J. M. Building Better Batteries. *Nature* **2008**, *451* (7179), 652−657.

(2) Kang, B.; Ceder, G. Battery Materials for Ultrafast Charging and Discharging. *Nature* **2009**, *458* (7235), 190−193.

(3) Lai, X.; Halpert, J. E.; Wang, D. Recent Advances in Micro-/Nano-Structured Hollow Spheres for Energy Applications: From Simple to Complex Systems. *Energy Environ. Sci.* **2012**, *5* (2), 5604−5618.

(4) Sun, Y. K.; Myung, S. T.; Park, B. C.; Prakash, J.; Belharouak, I.; Amine, K. High-Energy Cathode Material for Long-Life and Safe Lithium Batteries. *Nat. Mater.* **2009**, *8* (4), 320−324.

(5) Palacin, M. R. Recent Advances in Rechargeable Battery Materials: A Chemist's Perspective. *Chem. Soc. Rev.* **2009**, *38* (9), 2565−2575.

(6) Ammundsen, B.; Paulsen, J. Novel Lithium-Ion Cathode Materials Based on Layered Manganese Oxides. *Adv. Mater.* **2001**, *13* (12−13), 943−956.

(7) Wang, L.; Li, J. G.; He, X. M.; Pu, W. H.; Wan, C. R.; Jiang, C. Y. Recent Advances in Layered $LiNi_xCo_yMn_{1-x-y}O_2$ Cathode Materials for Lithium Ion Batteries. *J. Solid State Electrochem.* **2009**, *13* (8), 1157−1164.

(8) Cheng, F. Y.; Liang, J.; Tao, Z. L.; Chen, J. Functional Materials for Rechargeable Batteries. *Adv. Mater.* **2011**, *23* (15), 1695−1715.

(9) Jiang, Y.; Yang, Z.; Luo, W.; Hu, X. L.; Zhang, W. X.; Huang, Y. H. Facile Synthesis of Mesoporous $0.4Li_2MnO_3{\cdot}0.6LiNi_{2/3}Mn_{1/3}O_2$ Foams with Superior Performance for Lithium-Ion Batteries. *J. Mater. Chem.* **2012**, *22* (30), 14964−14969.

(10) Zhang, H. Z.; Qiao, Q. Q.; Li, G. R.; Ye, S. H.; Gao, X. P. Surface Nitridation of Li-Rich Layered $Li(Li_{0.17}Ni_{0.25}Mn_{0.58})O_2$ Oxide as Cathode Material for Lithium-Ion Battery. *J. Mater. Chem.* **2012**, *22* (10), 13104−13109.

(11) Xu, B.; Fell, C. R.; Chi, M. F.; Meng, Y. S. Identifying Surface Structural Changes in Layered Li-Excess Nickel Manganese Oxides in High Voltage Lithium Ion Batteries: A Joint Experimental and Theoretical Study. *Energy Environ. Sci.* **2011**, *4* (6), 2223−2233.

(12) Ito, A.; Li, D. C.; Sato, Y.; Arao, M.; Watanabe, M.; Hatano, M.; Horie, H.; Ohsawa, Y. Cyclic Deterioration and Its Improvement for Li-Rich Layered Cathode Material $Li[Ni_{0.17}Li_{0.2}Co_{0.07}Mn_{0.56}]O_2$. *J. Power Sources* **2010**, *195* (2), 567−573.

(13) Thackeray, M. M.; Johnson, C. S.; Vaughey, J. T.; Li, N.; Hackney, S. A. Advances in Manganese-Oxide 'Composite' Electrodes for Lithium-Ion Batteries. *J. Mater. Chem.* **2005**, *15*, 2257−2267.

(14) Yabuuchi, N.; Yoshii, K.; Myung, S. T.; Nakai, I.; Komaba, S. Detailed Studies of a High-Capacity Electrode Material for Rechargeable Batteries, $Li_2MnO_3{-}LiCo_{1/3}Ni_{1/3}Mn_{1/3}O_2$. *J. Am. Chem. Soc.* **2011**, *133* (12), 4404−4419.

(15) Armstrong, A. R.; Holzapfel, M.; Novák, P.; Johnson, C. S.; Kang, S.-H.; Thackeray, M. M.; Bruce, P. G. Demonstrating Oxygen Loss and Associated Structural Reorganization in the Lithium Battery Cathode $Li[Ni_{0.2}Li_{0.2}Mn_{0.6}]O_2$. *J. Am. Chem. Soc.* **2006**, *128* (26), 8694−8698.

(16) Arunkumar, T. A.; Wu, Y.; Manthiram, A. Factors Influencing the Irreversible Oxygen Loss and Reversible Capacity in Layered $Li[Li_{1/3}Mn_{2/3}]O_2{-}Li[M]O_2$ (M = $Mn_{0.5-y}Ni_{0.5-y}Co_{2y}$ and $Ni_{1-y}Co_y$) Solid Solutions. *Chem. Mater.* **2007**, *19* (12), 3067−3073.

(17) Jarvis, K. A.; Deng, Z.; Allard, L. F.; Manthiram, A.; Ferreira, P. J. Atomic Structure of a Lithium-Rich Layered Oxide Material for Lithium-Ion Batteries: Evidence of a Solid Solution. *Chem. Mater.* **2011**, *23* (16), 3614−3621.

(18) Lu, Z.; Dahn, J. R. Understanding the Anomalous Capacity of $Li/Li[Ni_xLi_{1/3-2x/3}Mn_{2/3-x/3}]O_2$ Cells Using *In Situ* X-ray Diffraction and Electrochemical Studies. *J. Electrochem. Soc.* **2002**, *149* (7), A815−A822.

(19) Thackeray, M. M.; Kang, S. H.; Johnson, C. S.; Vaughey, J. T.; Benedek, R.; Hackney, S. A. Li_2MnO_3-Stabilized $LiMO_2$ (M = Mn, Ni, Co) Electrodes for Lithium-Ion Batteries. *J. Mater. Chem.* **2007**, *17* (30), 3112−3125.

(20) He, W.; Qian, J.; Cao, Y.; Ai, X.; Yang, H. Improved Electrochemical Performances of Nanocrystalline $Li[Li_{0.2}Mn_{0.54}Ni_{0.13}Co_{0.13}]O_2$ Cathode Material for Li-Ion Batteries. *RSC Adv.* **2012**, *2* (8), 3423−3429.

(21) Zheng, J. M.; Li, J.; Zhang, Z. R.; Guo, X. J.; Yang, Y. The Effects of TiO_2 Coating on the Electrochemical Performance of $Li[Li_{0.2}Mn_{0.54}Ni_{0.13}Co_{0.13}]O_2$ Cathode Material for Lithium-Ion Battery. *Solid State Ionics* **2008**, *179* (27), 1794−1799.

(22) Wu, Y.; Murugan, A. V.; Manthiram, A. Surface Modification of High Capacity Layered $Li[Li_{0.2}Mn_{0.54}Ni_{0.13}Co_{0.13}]O_2$ Cathodes by $Alpo_4$. *J. Electrochem. Soc.* **2008**, *155* (9), A635−A641.

(23) Wang, Q. Y.; Liu, J.; Murugan, A. V.; Manthiram, A. High Capacity Double-Layer Surface Modified $Li[Li_{0.2}Mn_{0.54}Ni_{0.13}Co_{0.13}]O_2$ Cathode with Improved Rate Capability. *J. Mater. Chem.* **2009**, *19* (28), 4965−4972.

(24) Zheng, J. M.; Zhang, Z. R.; Wu, X. B.; Dong, Z. X.; Zhu, Z.; Yang, Y. The Effects of AlF_3 Coating on the Performance of $Li[Li_{0.2}Mn_{0.54}Ni_{0.13}Co_{0.13}]O_2$ Positive Electrode Material for Lithium-Ion Battery. *J. Electrochem. Soc.* **2008**, *155* (10), A775−A782.

(25) Sun, Y. K.; Lee, M. J.; Yoon, C. S.; Hassoun, J.; Amine, K.; Scrosati, B. The Role of AlF_3 Coatings in Improving Electrochemical Cycling of Li-Enriched Nickel-Manganese Oxide Electrodes for Li-Ion Batteries. *Adv. Mater.* **2012**, *24* (9), 1192−1196.

(26) Chen, Z.; Qin, Y.; Amine, K.; Sun, Y. K. Role of Surface Coating on Cathode Materials for Lithium-Ion Batteries. *J. Mater. Chem.* **2010**, *20* (36), 7606−7612.

(27) Shannon, R. D. Chemistry of Materials. *Acta Crystallogr.* **1976**, *32*, 751−767.

(28) He, W.; Yuan, D.; Qian, J.; Ai, X.; Yang, H.; Cao, Y. Enhanced High-Rate Capability and Cycling Stability of Na-Stabilized Layered $Li_{1.2}[Co_{0.13}Ni_{0.13}Mn_{0.54}]O_2$ Cathode Material. *J. Mater. Chem. A* **2013**, *1* (37), 11397−11403.

(29) Deng, Z. Q.; Manthiram, A. Influence of Cationic Substitutions on the Oxygen Loss and Reversible Capacity of Lithium-Rich Layered Oxide Cathodes. *J. Phys. Chem. C* **2011**, *115* (14), 7097−7103.

(30) Jiao, L. F.; Zhang, M.; Yuan, H. T.; Zhao, M.; Guo, J.; Wang, W.; Zhou, X. D.; Wang, Y. M. Effect of Cr Doping on the Structural, Electrochemical Properties of $Li[Li_{0.2}Ni_{0.2-x/2}Mn_{0.6-x/2}Cr_x]O_2$ (x = 0, 0.02, 0.04, 0.06, 0.08) as Cathode Materials for Lithium Secondary Batteries. *J. Power Sources* **2007**, *167* (1), 178−184.

(31) Lian, F.; Gao, M.; Qiu, W. H.; Axmann, P.; Wohlfahrt-Mehrens, M. Fe-Doping Effects on the Structural and Electrochemical Properties of $0.5Li_2MnO_3{\cdot}0.5LiMn_{0.5}Ni_{0.5}O_2$ Electrode Material. *J. Appl. Electrochem.* **2012**, *42* (6), 409−417.

(32) Park, J. H.; Lim, J.; Yoon, J.; Park, K. S.; Gim, J.; Song, J.; Park, H.; Im, D.; Park, M.; Ahn, D.; Paik, Y.; Kim, J. The Effects of Mo Doping on $0.3Li[Li_{0.33}Mn_{0.67}]O_2{\cdot}0.7Li[Ni_{0.5}Co_{0.2}Mn_{0.3}]O_2$ Cathode Material. *Dalton Trans.* **2012**, *41* (10), 3053−3059.

(33) Park, S. H.; Sun, Y. K. Synthesis and Electrochemical Properties of Layered $Li[Li_{0.15}Ni_{(0.275-x/2)}Al_xMn_{(0.575-x/2)}]O_2$ Materials Prepared by Sol−Gel Method. *J. Power Sources* **2003**, *119−121*, 161−165.

(34) Song, B.; Lai, M. O.; Lu, L. Influence of Ru Substitution on Li-Rich $0.55Li_2MnO_3{\cdot}0.45LiNi_{1/3}Co_{1/3}Mn_{1/3}O_2$ Cathode for Li-Ion Batteries. *Electrochim. Acta* **2012**, *80*, 187−195.

DOI: 10.1021/acsami.5b03125
ACS Appl. Mater. Interfaces 2015, 7, 13014−13021

(35) Xu, H.; Deng, S.; Chen, G. Improved Electrochemical Performance of $Li_{1.2}Mn_{0.54}Ni_{0.13}Co_{0.13}O_2$ by Mg Doping for Lithium Ion Battery Cathode Material. *J. Mater. Chem. A* **2014**, *2* (36), 15015−15021.
(36) Xiao, L.; Zhao, Y.; Yang, Y.; Cao, Y.; Ai, X.; Yang, H. Enhanced Electrochemical Stability of Al-Doped $LiMn_2O_4$ Synthesized by a Polymer-Pyrolysis Method. *Electrochim. Acta* **2008**, *54* (2), 545−550.
(37) Yu, L.; Yang, H.; Ai, X.; Cao, Y. Structural and Electrochemical Characterization of Nanocrystalline $Li[Li_{0.12}Ni_{0.32}Mn_{0.56}]O_2$ Synthesized by a Polymer-Pyrolysis Route. *J. Phys. Chem. B* **2005**, *109*, 1148−1154.
(38) Kang, S. H.; Kempgens, P.; Greenbaum, S.; Kropf, A. J.; Amine, K.; Thackeray, M. M. Interpreting the Structural and Electrochemical Complexity of $0.5Li_2MnO_3{\cdot}0.5LiMO_2$ Electrodes for Lithium Batteries ($M = Mn_{0.5-x}Ni_{0.5-x}Co_{2x}$, $0 \le x \le 0.5$). *J. Mater. Chem.* **2007**, *17* (20), 2069−2077.
(39) Park, S.; Kang, S.; Johnson, C.; Amine, K.; Thackeray, M. Lithium−Manganese−Nickel-Oxide Electrodes with Integrated Layered−Spinel Structures for Lithium Batteries. *Electrochem. Commun.* **2007**, *9* (2), 262−268.
(40) Yu, L.; Qiu, W.; Lian, F.; Huang, J.; Kang, X. Understanding the Phenomenon of Increasing Capacity of Layered $0.65Li[Li_{1/3}Mn_{2/3}]O_2{\cdot}0.35Li(Ni_{1/3}Co_{1/3}Mn_{1/3})O_2$. *J. Alloys Compd.* **2009**, *471* (1−2), 317−321.
(41) Kim, J. Synthesis and Electrochemical Behavior of $Li[Li_{0.1}Ni_{0.35-x/2}Co_xMn_{0.55-x/2}]O_2$ Cathode Materials. *Solid State Ionics* **2003**, *164* (1−2), 43−49.
(42) Luo, W.; Zhou, F.; Zhao, X.; Lu, Z.; Li, X.; Dahn, J. R. Synthesis, Characterization, and Thermal Stability of $LiNi_{1/3}Mn_{1/3}Co_{1/3-z}Mg_zO_2$, $LiNi_{1/3-z}Mn_{1/3}Co_{1/3}Mg_zO_2$, and $LiNi_{1/3}Mn_{1/3-z}Co_{1/3}Mg_zO_2$. *Chem. Mater.* **2010**, *22* (3), 1164−1172.
(43) Luo, W.; Li, X.; Dahn, J. R. Synthesis and Characterization of Mg Substituted $LiCoO_2$. *J. Electrochem. Soc.* **2010**, *157* (7), A782−A790.
(44) Thackeray, M. M.; Kang, S. H.; Johnson, C. S.; Vaughey, J. T.; Benedek, R.; Hackney, S. A. Li_2MnO_3-Stabilized $LiMO_2$ (M = Mn, Ni, Co) Electrodes for Lithium-Ion Batteries. *J. Mater. Chem.* **2007**, *17* (30), 3112−3125.
(45) Lu, Z. H.; Dahn, J. R. Understanding the Anomalous Capacity of $Li/Li[Ni_xLi_{1/3-2x/3}Mn_{2/3-x/3}]O_2$ Cells Using *In Situ* X-ray Diffraction and Electrochemical Studies. *J. Electrochem. Soc.* **2002**, *149* (7), A815−A822.
(46) He, W.; Qian, J.; Cao, Y.; Ai, X.; Yang, H. Improved Electrochemical Performances of Nanocrystalline $Li[Li_{0.2}Mn_{0.54}Ni_{0.13}Co_{0.13}]O_2$ Cathode Material for Li-Ion Batteries. *RSC Adv.* **2012**, *2* (8), 3423−3429.
(47) Venkatraman, S.; Manthiram, A. Comparison of the Phase Relationships of Chemically Delithiated Layered $Li_{1-x}Co_{1-y}M_yO_2$ (M = Al and Mg) Oxides. *Solid State Ionics* **2005**, *176* (3−4), 291−298.
(48) Kim, G.-H.; Myung, S.-T.; Kim, H.-S.; Sun, Y.-K. Synthesis of Spherical $Li[Ni_{(1/3-z)}Co_{(1/3-z)}Mn_{(1/3-z)}Mg_z]O_2$ as Positive Electrode Material for Lithium-Ion Battery. *Electrochim. Acta* **2006**, *51* (12), 2447−2453.
(49) Li, D.; Sasaki, Y.; Kobayakawa, K.; Sato, Y. Morphological, Structural, and Electrochemical Characteristics of $LiNi_{0.5}Mn_{0.4}M_{0.1}O_2$ (M = Li, Mg, Co, Al). *J. Power Sources* **2006**, *157* (1), 488−493.
(50) Wu, F.; Zhang, X.; Zhao, T.; Li, L.; Xie, M.; Chen, R. Multifunctional $Alpo_4$ Coating for Improving Electrochemical Properties of Low-Cost $Li[Li_{0.2}Fe_{0.1}Ni_{0.15}Mn_{0.55}]O_2$ Cathode Materials for Lithium-Ion Batteries. *ACS Appl. Mater. Interfaces* **2015**, *7* (6), 3773−3781.

DOI: 10.1021/acsami.5b03125
ACS Appl. Mater. Interfaces 2015, 7, 13014−13021